Sensors and Actuators A 248 (2016) 184–192

Contents lists available at ScienceDirect

Sensors and Actuators A: Physical

journal homepage: www.elsevier.com/locate/sna

High-speed vertical positioning stage with integrated dual-sensor arrangement

Yuen K. Yong*, Andrew J. Fleming

School of Electrical Engineering and Computer Science, The University of Newcastle, Callaghan, NSW 2308, Australia

ARTICLE INFO

Article history:
Received 28 April 2016
Received in revised form 30 June 2016
Accepted 30 June 2016
Available online 11 July 2016

Keywords:
Piezoresistive
Strain sensor
Piezoelectric
Force sensor
Nanopositioning
Control
High-speed
AFM

ABSTRACT

This article presents a novel vertical positioning stage with a dual-sensor arrangement suitable for scanning probe microscopy. The stage has a travel range of 8.4 μm and a first resonance frequency of 24 kHz in the direction of travel. The sensor arrangement consists of an integrated piezoelectric force sensor and laminated piezoresistive strain sensor. The piezoelectric force sensor exhibits extremely low noise and introduces a zero into the dynamics which allows the use of integral force feedback. This control method provides excellent damping performance and guaranteed stability. The piezoresistive sensor is used for tracking control with an analog PI controller which is shown to be an approximate inverse of the damped system. The resulting closed-loop system has a bandwidth is 11.4 kHz and 6σ-resolution of 3.6 nm, which is ideal for nanopositioning and atomic force microscopy (AFM) applications. The proposed vertical stage is used to replace the vertical axis of a commercial AFM. Scans are performed in constant-force contact mode with a tip velocity of 0.2 mm/s, 1 mm/s and 2 mm/s. The recorded images contain negligible artefacts due to insufficient vertical bandwidth.

1. Introduction

Compact, high-bandwidth nanopositioning systems have been employed in a wide range of applications, including precision alignment of fiber optics [1], scanning probe microscopy [2–5], beam steering systems [6] and cavity ring-down spectroscopy in optical applications [7,8]. Piezoelectric stack actuators are used in these precision systems due to the high force and stiffness. However, piezoelectric stack actuators exhibit hysteresis over a large range and creep at low frequencies. These nonlinearities can cause tracking errors greater than 20%.

Many forms of feedback and feedforward control have been applied to eliminate vibration, hysteresis and creep [9–11]. Inversion-based feedforward techniques [11–13] can be used to suppress the sharp resonance behavior and improve the tracking performance of nanopositioning systems without the need of a sensor. However, the main disadvantage of feedforward control is the need for an accurate model and a stable resonance frequency. A nonlinear model, which may be computationally demanding to invert, is also required for hysteresis and creep compensation.

Sensor-based feedback control is one of the most commonly used techniques for controlling piezoelectric systems [11,13–16]. This approach is simple, insensitive to modeling error, and effectively reduces nonlinearity. Damping controllers, such as integral resonant control [17–19], positive position feedback [20–23], resonant control [24] and polynomial-based controller [25] have been used to suppress resonances and reduce the bandwidth limitations imposed by mechanical resonances. However, when a damped system is included in an integral tracking loop, the closed-loop system is still limited by a low gain margin [26]. Moreover, the wide bandwidth of a damping controller can introduce sensor-induced positioning noise to the system.

Capacitive sensors are among the most popular sensors used in nanopositioning systems owing to their low noise, high resolution and relatively low cost [27]. They can be easily installed in the lateral axis of nanopositioning systems as shown in Fig. 1(a). However, for the vertical axis of a compact nanopositioner, the installation of the sensor becomes challenging. As shown in Fig. 1(b), additional mass on the moving platform may be needed to serve as a target for the sensor, which increases the physical size and reduces the resonance frequency.

In this work, a dual-sensor system is proposed for controlling vibration and nonlinearity in a piezoelectric driven, high-speed vertical stage. The technique utilizes a piezoelectric force sensor and a piezoresistive strain sensor to estimate displacement. The two sensors are bonded to the piezoelectric stack actuator directly which

* Corresponding author.
E-mail addresses: yuenkuan.yong@newcastle.edu.au (Y.K. Yong), andrew.fleming@newcastle.edu.au (A.J. Fleming).

http://dx.doi.org/10.1016/j.sna.2016.06.042
0924-4247/

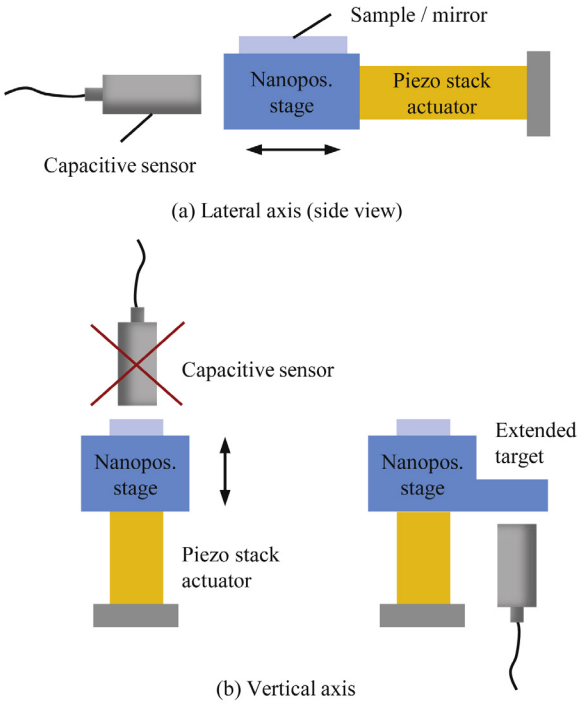

Fig. 1. Installation of a capacitive sensor on the lateral and vertical axes of a nanopositioner.

allows for an extremely compact design. The piezoelectric force sensor provides a wide bandwidth with low noise at high frequencies [28,29]. Although piezoelectric force sensors have excellent AC properties, the sensitivity is temperature dependent and they are not suitable for low-frequency measurements due to the capacitive source impedance which imposes a first-order high-pass response. To overcome these limitations, a piezoresistive strain sensor is used for tracking control and to augment the force sensor at frequencies below 10 Hz. Piezoresisitive strain sensors can be directly bonded to a stack actuator without affecting the dynamic performance. The sensitivity of piezoresistive sensors is typically two orders of magnitude greater than metal foil strain sensors so sub-nanometer resolution can be achieved at kHz bandwidths [27].

The performance of the proposed vertical system is demonstrated on a commercial AFM where the vertical axis of the AFM is replaced by the high-speed vertical stage. Many common modes of scanning probe microscopy (SPM), such as constant-force AFM and constant-current scanning tunneling microscopy, require a vertical feedback system to regulate the interaction force between tip and sample. A major speed limitation in these modes is the vertical feedback bandwidth [2,3,30–32]. During a high-speed scan, an AFM system with a low vertical feedback bandwidth is unable to track sharp features in a sample topography. This leads to the "smudging" feature edges in the image [13,30]. The most commonly used vertical feedback controller in an AFM is an integral controller. The vertical bandwidth can therefore be estimated as ω_n/P, where ω_n is the resonance frequency and P is the peak magnitude [33]. By increasing the resonance frequency of the vertical stage, and actively damping the resonance using force-feedback, the maximum vertical feedback bandwidth can be improved significantly.

The remainder of the paper proceeds as follows. Section 2 presents the design of the vertical stage and the preload mechanism. This section also discusses the design of the actuator and sensor arrangement. Feedback control strategies using the dual-sensor arrangement are presented in Section 3. Experimental results can be found in Section 4. Section 5 reports the position noise of the sensors and closed-loop system. The vertical system is then used for Atomic Force Microscopy (AFM) in Section 6. The article is concluded in Section 7.

2. High-speed vertical stage design

Fig. 2 illustrates the proposed high-speed vertical stage which consists of four sets of leaf-spring flexures arranged orthogonally. These flexures allow the central platform to move vertically while simultaneously restraining the lateral motion. A 7 mm × 7 mm × 11.5 mm piezoelectric stack actuator is used to deform the flexures elastically and to drive the central platform.

2.1. Actuator and sensors

The piezoelectric stack actuator is constructed from four 2-mm plate stacks (NOLIAC NAC2021) bonded in series to a 2-mm NAC2021 force sensor as shown in Fig. 3. A 0.5-mm ceramic plate is used to separate the sensor and actuator in order to minimize Poisson coupling from the actuator to sensor. Two more ceramic plates are glued to each end of the actuator respectively to electrically isolate the actuator from the nanopositioner. The piezoresistive strain sensor is a Micron Instruments SSGH-060-033-1000PB half-bridge which is glued to the side of the actuator for displacement measurement.

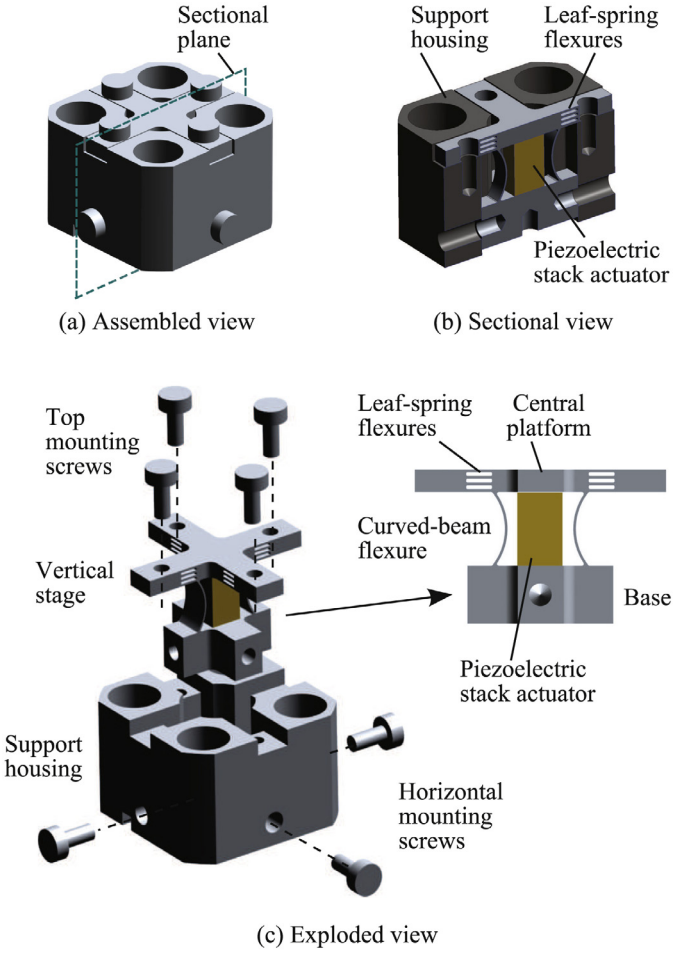

Fig. 2. High-speed vertical stage. (a) Assembly view showing the vertical stage being mounted to its support housing. (b) Sectional view showing the vertical stage, support housing and piezoelectric stack actuator. (c) Exploded view of the vertical stage.

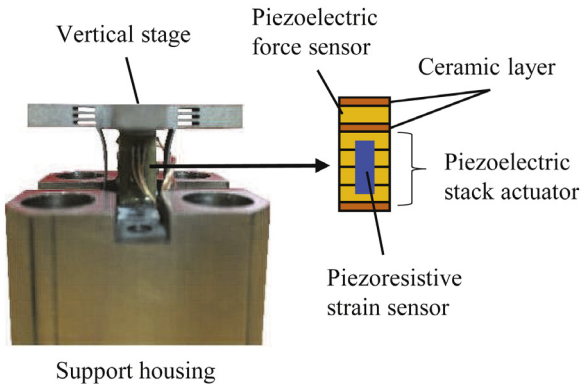

Fig. 3. Piezoelectric stack actuator with force and piezoresistive strain sensors.

2.2. Preloading and installation of piezoelectric stack actuator

To prevent damage due to tensile stress, a sufficient preload is required to compensate for inertial forces. Many high-speed nanopositioner systems uses flexures to preload piezoelectric stack actuators [3,14,31,34]. These flexures are also used to provide the requisite stiffness for high-speed operation. However, due to the high stiffness, it is difficult to achieve a measured preload during installation. For instance, to deform a group of flexures with a combined stiffness of 10 N/μm [14,34] by 0.3 mm, a pulling force of 3000 N is required. To provide this pulling force, a specially designed pulley system or a high-force preloading tool may be needed. The stiffness of flexures may be reduced to simplify the installation process but this degrades the dynamic performance.

The proposed vertical stage includes two curved flexures shown in Fig. 2 which simplify the actuator installation and preloading. The low stiffness of the curved flexures permits installation of the actuator with tens of Newtons of force. This preload force can be practically applied using precision screws. Details of the curved flexure design and the preloading procedure can be found in [35].

3. Feedback control strategy

Due to the capacitive source impedance of the piezoelectric force sensor, the dynamics resemble a high-pass filter with a cut-off frequency of $1/RC_p$, where R is the input impedance of the instrumentation and C_p is the capacitance of the sensor. In the experimental setup, the capacitance and resistance are 158 nF and 100 MΩ which result in a high-pass cut-off frequency of 0.01 Hz. The vertical stage is considered to be a single-input two-output (SITO) system described by

$$\begin{bmatrix} d \\ f \end{bmatrix} = \begin{bmatrix} G_{da} \\ G_{fa} \end{bmatrix} V_a, \tag{1}$$

where V_a is the applied input voltage, d is the piezoresistive strain sensor measurement, and f is the piezoelectric force sensor measurement. The sensitivity of the piezoresistive strain sensor was measured to be 42 mV/μm, which was approximately 5% of the force sensor. For simplicity, the strain sensor signal was amplified so that the sensitivity was equal to the force sensor, that is 1.594 V/μm.

The transfer functions from V_a to d and f were identified to be

$$G_{da} = \frac{2.48 \times 10^{10}}{s^2 + 22,060s + 2.483 \times 10^{10}} \tag{2}$$

$$G_{fa} = \frac{2.789s^2 + 5250s + 2.048 \times 10^{10}}{s^2 + 22,060s + 2.483 \times 10^{10}}. \tag{3}$$

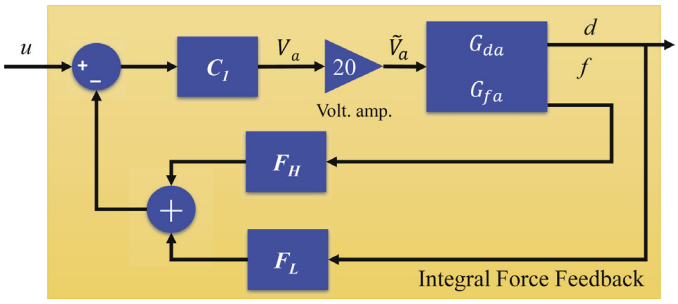

Fig. 4. The integral force feedback damping control loop.

3.1. Integral force feedback

To suppress the resonance of the vertical stage, an integral force feedback (IFF) controller is implemented as shown in Fig. 4. A pair of complementary filters F_L and F_H are used to substitute f for d at frequencies below the cut-off frequency f_c, chosen to be 10 Hz. F_L and F_H are first-order filters with transfer functions

$$F_L = \frac{2\pi f_c}{s + 2\pi f_c} \quad \text{and} \quad F_H = \frac{s}{s + 2\pi f_c}. \tag{4}$$

The IFF loop consists of the plant G_{fa} and an integrator $C_1(s) = \alpha/s$ [26]. The closed-loop response of the damping loop from u to d is

$$G_{du} = \frac{C_1 G_{da}}{1 + C_1 G_{fa}}. \tag{5}$$

Due to the force sensor, the transfer function G_{fa} exhibits zero-pole interlacing pattern where the phase response lies between 0° and 180°. Such systems are known as negative imaginary systems and have guaranteed stability with an integral controller [36]. Using the root-locus method, an integral gain of $\alpha = 14{,}000$ was found to achieve optimal damping.

3.2. Tracking control

An outer tracking control loop is implemented using the piezoresistive strain sensor as illustrated in Fig. 5. The damping control loop G_{du} features an additional real axis pole introduced by the IFF controller [37]. This additional pole can be approximately inverted by placing a zero at a similar frequency [37]. Since the desired loop gain is integral action, a suitable controller is

$$C_2(s) = \frac{k_i(s + w_z)}{sw_z}, \tag{6}$$

where k_i is an integral gain, and w_z is the frequency of the additional pole which can be found experimentally, by examining the pole-zero map of G_{du} or by the Cardano's method [37]. C_2 is a PI controller with a parameterized zero location. In the experimental setup, w_z was found to be 11,800 rad/s. A tracking controller gain

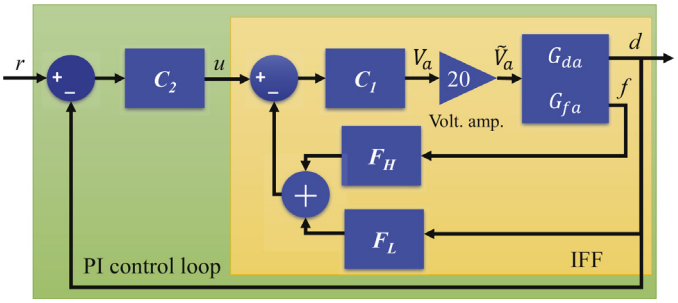

Fig. 5. The reference tracking and damping control loops where C_1 is the integral force feedback controller and C_2 is the PI controller.

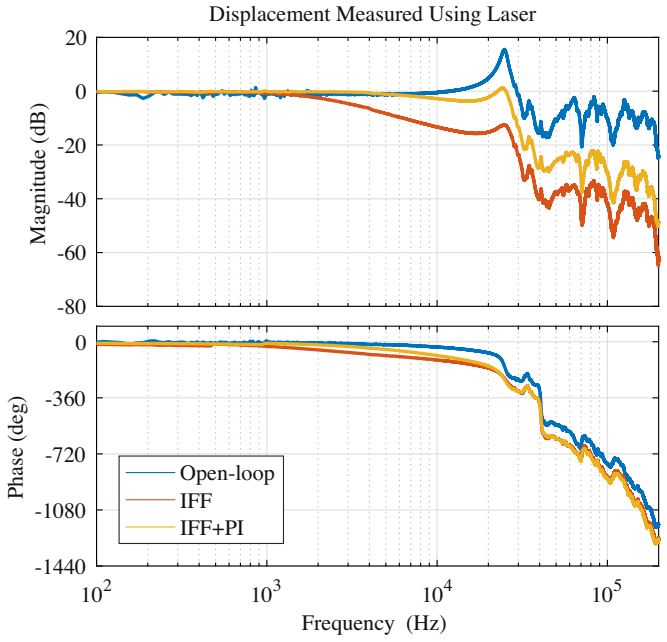

Fig. 6. Normalized frequency responses of the vertical stage measured using a laser vibrometer.

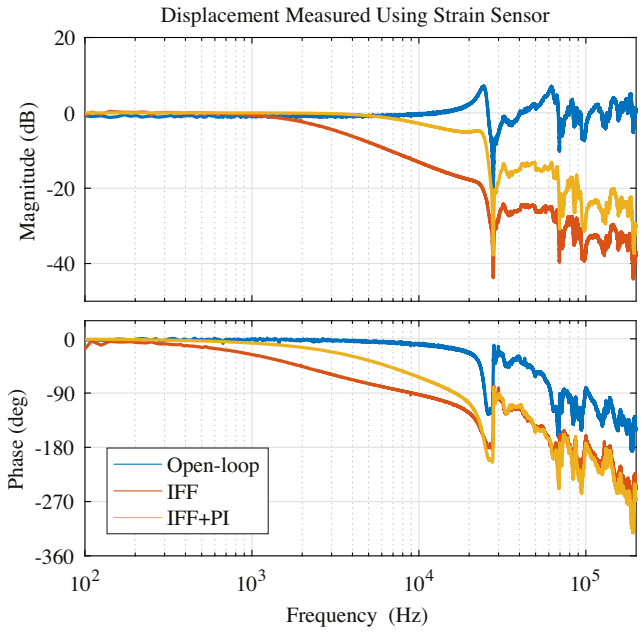

Fig. 7. Normalized frequency responses of the vertical stage measured using piezoresistive strain sensor.

of $k_i = 25{,}000$ was chosen which results in a gain margin of 7.2 dB and phase margin of 72°.

4. Experimental results

A Polytec PSV-300 laser scanning vibrometer was used to measure the open- and closed-loop frequency response of system. The open-loop frequency responses were measured from the applied voltage V_a to the displacement d. The damping loop responses (IFF) were measured from the signal u to d, and the closed-loop tracking responses (IFF + PI) were measured from r to d. Results measured by the laser and the strain sensor are plotted in Figs. 6 and 7 respectively. With the implementation of the IFF and PI controllers, the magnitude of the first resonance mode is suppressed by 16 dB. The 3-dB bandwidth of the closed-loop system is 11.4 kHz which is approximately 50% of the first resonance frequency. This is an excellent result given that the controller is second order and implemented by analog circuit.

To evaluate the effect of hysteresis, the vertical stage was driven at full range (8.4 μm) with a sinusoidal input at 10 Hz. The open- and closed-loop hysteresis plots are shown in Fig. 8. The hysteresis is observed to be eliminated at this frequency.

5. Noise and resolution estimation

In this work, the foremost sources of noise are the strain and force sensor. The noise density function of the piezoresistive strain and piezoelectric force sensors are plotted in Fig. 9. The piezoelectric force sensor exhibits low noise at high frequencies but is dominated by integrated current noise from the instrumentation at low frequencies, which results in $1/f^2$ characteristic. The piezoresistive strain sensor has a higher noise density of 1.5 pm/$\sqrt{\text{Hz}}$. However, at low-frequencies, the piezoresistive sensor exhibits a $1/f$ characteristic which is due to semiconductor noise. This $1/f$ characteristic results in significantly less DC to 10-Hz noise compared to the $1/f^2$ characteristic of the force sensor.

The total closed-loop positioning noise is estimated using the time-domain applied voltage method described in reference [38]. In this method, the total positioning noise can be estimated by

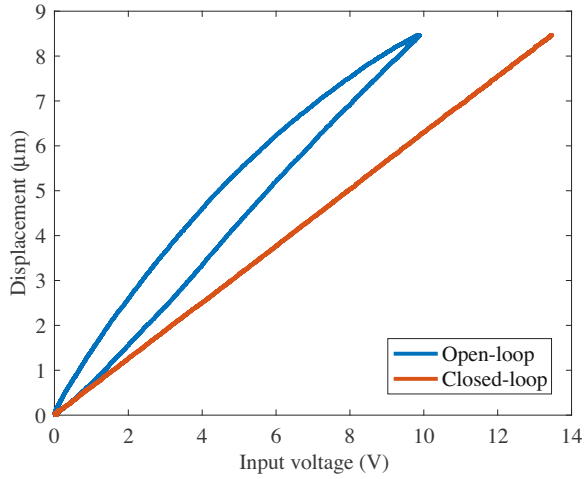

Fig. 8. Hysteresis plots of the system in open- and closed-loop.

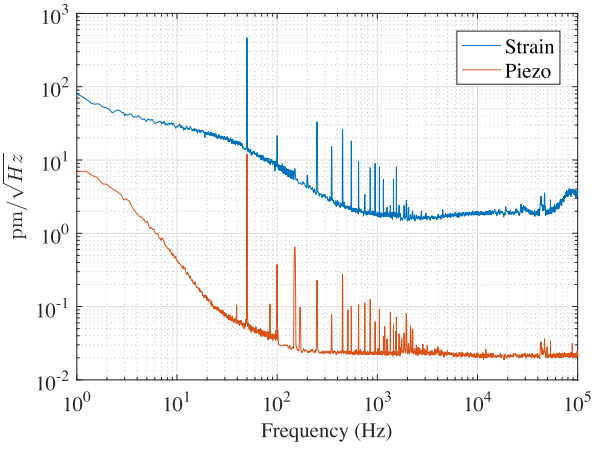

Fig. 9. Noise density function of the piezoresistive strain sensor, piezoelectric force sensor and the closed-loop system.

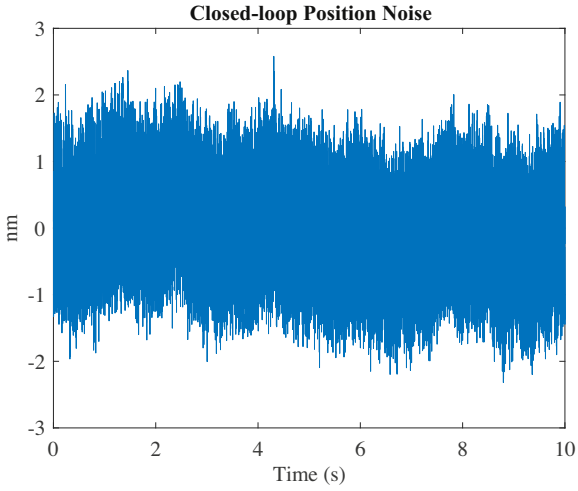

Fig. 10. Closed-loop position noise measured in time-domain.

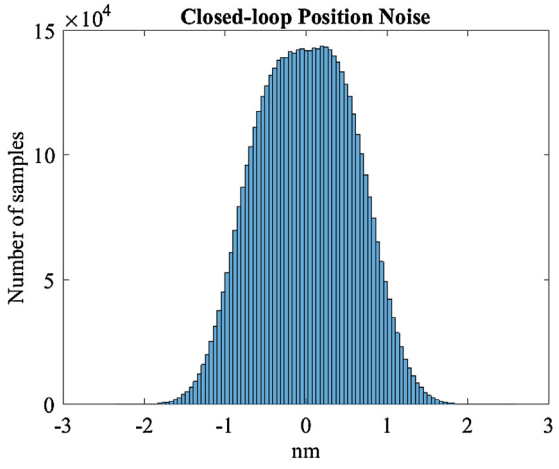

Fig. 11. Distribution of the closed-loop position noise.

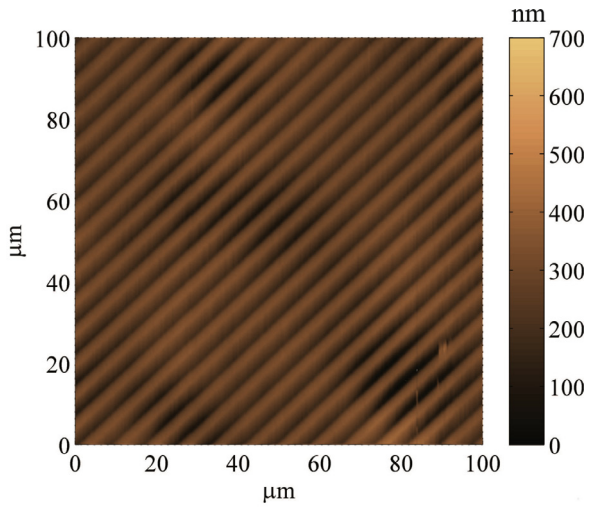

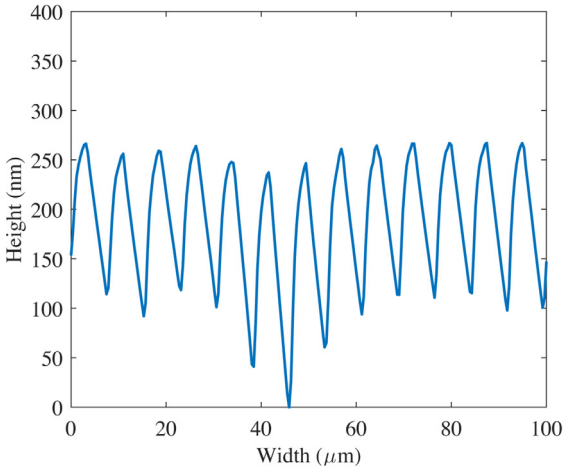

Fig. 13. The topography (top) and profile (bottom) of the sample obtained using the commercial AFM at 1 Hz scan rate.

measuring the applied voltage $\tilde{V}_a$ to the plant in closed-loop (see Fig. 5), and post-filtering it by the plant dynamics. A 10 s period of the applied voltage was recorded at 512 kHz. An SR560 low-noise preamplifier was used to amplify the AC component of the signal by 20 and to filter the signal with a first-order high-pass filter at 0.016 Hz and second-order low-pass filter at 30 kHz. The recorded signal $\tilde{V}_a$ was then filtered by the model G_{da} using `lsim` in Matlab. The closed-loop position noise and its approximately Gaussian distribution are plotted in Figs. 10 and 11. The position noise has an RMS value of 0.6 nm and a 6σ-resolution of 3.6 nm. This resolution can be compared to that achievable with a state of the art MicroSense 6810 capacitive sensor with a noise density of

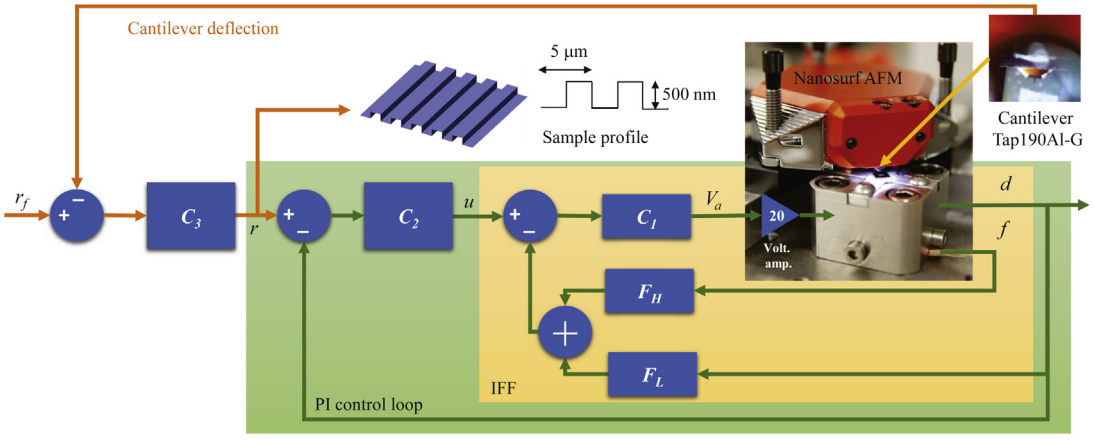

Fig. 12. Experimental setup for performing constant-force contact-mode AFM. The high-speed vertical stage is mounted under the Nanosurf AFM. C_3 is an integral controller with a gain of 26,000. r_f is the force set-point of 35 nN.

10 pm/$\sqrt{\text{Hz}}$ and a $1/f$ noise corner frequency of 100 Hz. In ideal conditions (ignoring 50 Hz noise), the capacitive sensor would provide a predicted closed-loop 6σ-resolution of approximately 2.6 nm, which is comparable to the resolution achieved with the proposed sensor arrangement.

$$6\sigma\text{-resolution} = 6\sqrt{A}\sqrt{f_{nc}\ln\frac{f_h}{f_l} + k_e f_h} \quad (7)$$

where A is the noise density, f_{nc} is the $1/f$ noise corner frequency, f_l and f_h are the lower and upper bounds of the bandwidth of interest, and $k_e = 1.57$ is a correction factor that accounts for the finite roll-off of the system.

6. AFM imaging

In this section, the performance of the proposed closed-loop vertical system is evaluated for AFM applications. The AFM

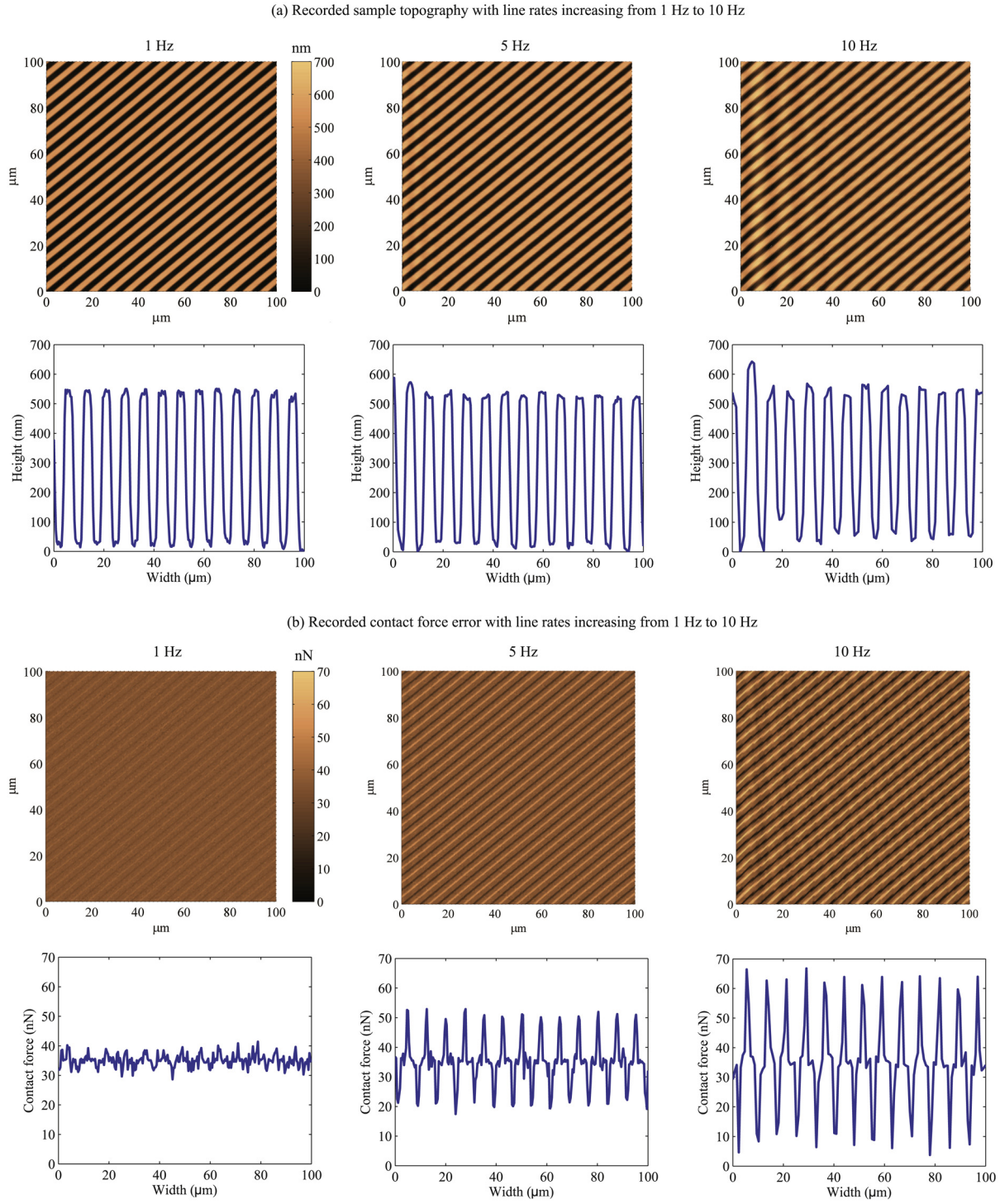

Fig. 14. AFM images and contact force errors obtained using the proposed high-speed vertical stage for line rates of 1 Hz, 5 Hz and 10 Hz. The quality of these images are much superior compared to that of the commercial AFM in Fig. 13.

experiments were conducted in constant-force contact-mode with a HS-500MG sample grating which has a rectangular profile of 5 μm period and 500 nm height (see Fig. 12). A BudgetSensors Tap190Al-G cantilever with a resonance frequency of 190 kHz was used to probe the sample. The contact force was regulated at 35 nN while scanning a sample area of 100 μm × 100 μm with 256 × 256 pixels resolution.

Firstly, the Nanosurf AFM which has a closed-loop vertical bandwidth of 45 Hz is used to interrogate the sample at 1 Hz line rate. Fig. 13 shows the resulting topography image and the single-line profile of the grating. The shape and height of the profile are heavily distorted by the limited bandwidth of the vertical feedback loop. In constant-force imaging modes, the vertical feedback controller regulates the contact force in response to the topography signal which enters the loop as an input disturbance. For a 100 μm × 100 μm scan area at 1 Hz line rate, the tip velocity is v_{tip} = 200 μm/s. Assuming the sample has a sinusoidal profile with periodicity λ, the required feedback bandwidth is [4]

$$f_B \geq \frac{v_{tip}}{\lambda}. \tag{8}$$

For λ = 5 μm, f_B is required to be at least 40 Hz. Note that the above estimation is for a sinusoidal profile, significantly higher bandwidths are required to track topographies with step changes.

The same experiments were repeated where the vertical axis of the AFM was replaced by the proposed vertical stage, as shown in Fig. 12. C_3 is an integral controller used to regulate the contact force at 35 nN. The integral gain was set to 26,000. As a result, the closed-loop vertical bandwidth of the AFM was measured to be 9 kHz. The AFM images obtained at 1 Hz, 5 Hz and 10 Hz line rates are plotted in Fig. 14. The corresponding tip velocities were 0.2 mm/s, 1 mm/s and 2 mm/s respectively. No imaging artefacts due to the vertical

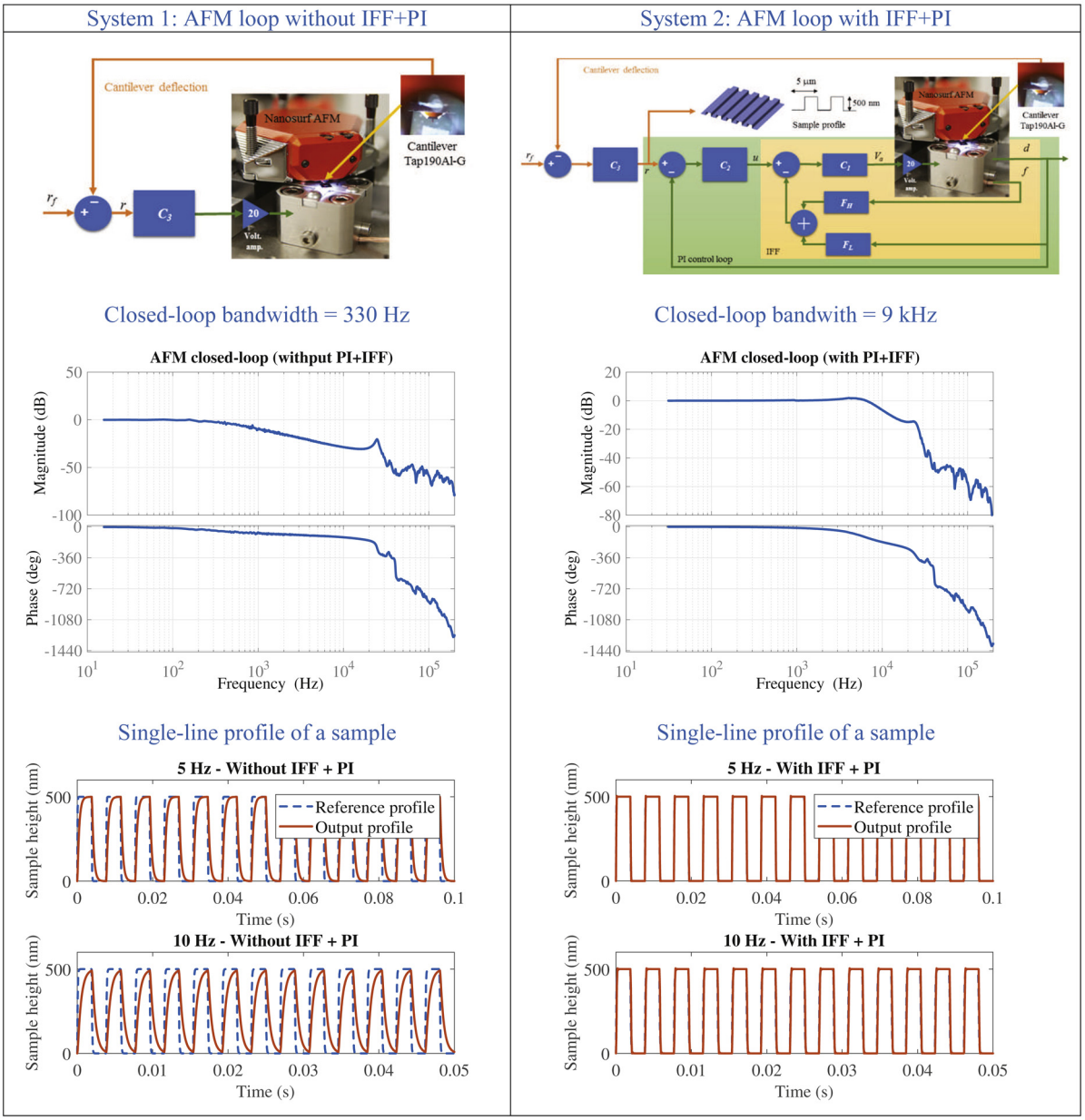

Fig. 15. Tracking performances of an AFM closed-loop system without the IFF + PI inner loop (left column); and with the IFF + PI inner loop (right column). First row: system block diagram. Middle row: frequency response of each system, indicating their closed-loop bandwidths. Last row: tracking of a single-line profile of a sample with rectangular features at 5 Hz and 10 Hz line rates.

bandwidth can be observed. However, at the higher scan-rates, distortion due to the dynamics of the lateral axes can be observed. Oscillations appear in the recorded images when the lateral scan rate is increased to 5 Hz and 10 Hz respectively. These oscillations are more noticeable at the start of each scan line (left side of the image) due to the fast dynamics content of the lateral triangular reference. Similar vibration-induced artifacts have been described in [13,14,18,34].

To illustrate the benefits of actively damping the vertical stage in AFM applications, Fig. 15 compares the simulated vertical feedback bandwidth with and without active damping. In both cases, the integral tracking controller (C_3) was tuned to provide a 10 dB gain-margin. The system without active damping has a 3-dB bandwidth of 330 Hz, while the system with active damping has a bandwidth of 9 kHz. Therefore, if the vertical stage has a significant resonance peak, active damping can significantly increase the performance while retaining a simple vertical feedback controller. It is advantageous to retain a simple vertical feedback controller as this is regularly retuned after a change of imaging mode, sample, or cantilever.

7. Conclusions

This article presents a high-speed vertical stage with an integrated dual-sensor arrangement for vibration and tracking control. The dual-sensor arrangement of a piezoelectric force sensor and piezoresistive strain sensor offers a compact alternative to capacitive and optical sensors. The integral force feedback damping controller and PI tracking controller provided a closed-loop bandwidth of 11.4 kHz, which is approximately 50% of the first resonance frequency. The closed-loop 6σ positioning resolution was measured to be 3.6 nm, which is comparable to that achievable with a high-performance capacitive sensor.

When the proposed stage was used to replace the vertical axis of a commercial AFM, the closed-loop vertical feedback bandwidth was increased from 43 Hz to 9 kHz. AFM images recorded at velocities of 0.2 mm/s, 1 mm/s and 2 mm/s demonstrate the elimination of imaging artefacts associated with insufficient vertical feedback bandwidth.

Acknowledgments

This work was supported by the Australian Research Council DECRA Project DE130100879, Discovery Project DP150103521 and the Future Fellowship FT130100543.

References

[1] Z. Wang, L. Chen, L. Sun, An integrated parallel micromanipulator with flexure hinges for optical fiber alignment, in: International Conference on Mechatronics and Automation, 2007. ICMA 2007, 2007, pp. 2530–2534, http://dx.doi.org/10.1109/ICMA.2007.4303954.
[2] Y.K. Yong, S.O.R. Moheimani, A compact XYZ scanner for fast atomic force microscopy in constant force contact mode, in: IEEE/ASME International Conference on Advanced Intelligent Mechatronics, Montreal, Canada, 2010, pp. 225–230.
[3] B.J. Kenton, A.J. Fleming, K.K. Leang, Compact ultra-fast vertical nanopositioner for improving scanning probe microscope scan speed, Rev. Sci. Instrum. 82 (12) (2011) 123703.
[4] T. Ando, High-speed atomic force microscopy coming of age, Nanotechnology 23 (6) (2012) 062001.
[5] G. Schitter, K.J. Astrom, B.E. DeMartini, P.J. Thurner, K.L. Turner, P.K. Hansma, Design and modeling of a high-speed AFM-scanner, IEEE Trans. Control Syst. Technol. 15 (5) (2007) 906–915.
[6] J.J. Gorman, N.G. Dagalakis, B.G. Boone, Multi-loop control of nanopositioning mechanism for ultra-precision beam steering, in: Proc. SPIE Conf. Free-space Laser Communication and Active Laser Illumination III, vol. 5160, San Diego, CA, 2003, pp. 170–181.
[7] G. Berden, R. Peeters, G. Meijer, Cavity ring-down spectroscopy: experimental schemes and applications, Int. Rev. Phys. Chem. 19 (4) (2000) 565–607, http://dx.doi.org/10.1080/014423500750040627.
[8] I. Debecker, A. Mohamed, D. Romanini, High-speed cavity ringdown spectroscopy with increased spectral resolution by simultaneous laser and cavity tuning, Opt. Express 13 (8) (2005) 2906–2915, http://dx.doi.org/10.1364/OPEX.13.002906.
[9] K.K. Leang, S. Devasia, Feedback-linearized inverse feedforward for creep, hysteresis, and vibration compensation in piezoactuators, IEEE Control Syst. Technol. 15 (5) (2007) 927–935 (Special issue on dynamics and control of micro- and nano-scale systems).
[10] D. Croft, G. Shedd, S. Devasia, Creep, hysteresis, and vibration compensation for piezoactuators: atomic force microscopy application, J. Dynam. Syst. Meas. Control 123 (1) (2001) 35–43.
[11] S. Devasia, E. Eleftheriou, S.O.R. Moheimani, A survey of control issues in nanopositioning, IEEE Trans. Control Syst. Technol. 15 (2007) 802–823.
[12] K. Leang, Q. Zou, S. Devasia, Feedforward control of piezoactuators in atomic force microscope systems, IEEE Control Syst. Mag. 9 (1) (2009) 70–82.
[13] Y.K. Yong, S.O.R. Moheimani, B.J. Kenton, K.K. Leang, Invited review article: high-speed flexure-guided nanopositioning: mechanical design and control issues, Rev. Sci. Instrum. 83 (12) (2012) 121101.
[14] B.J. Kenton, K.K. Leang, Design and control of a three-axis serial-kinematic high-bandwidth nanopositioner, IEEE/ASME Trans. Mechatron. 17 (2) (2012) 356–368.
[15] T. Tuma, W. Haeberle, H. Rothuizen, J. Lygeros, A. Pantazi, A. Sebastian, Dual-stage nanopositioning for high-speed scanning probe microscopy, IEEE/ASME Trans. Mechatron. 19 (3) (2014) 1035–1045, http://dx.doi.org/10.1109/TMECH.2013.2266481.
[16] S.O.R. Moheimani, Invited review article: accurate and fast nanopositioning with piezoelectric tube scanners: emerging trends and future challenges, Rev. Sci. Instrum. 79 (7) (2008) 071101.
[17] S.S. Aphale, A.J. Fleming, S.O.R. Moheimani, Integral resonant control of collocated smart structures, Smart Mater. Struct. 16 (2007) 439–446.
[18] A.J. Fleming, S. Aphale, S.O.R. Moheimani, A new method for robust damping and tracking control of scanning probe microscope positioning stages, IEEE Trans. Nanotechnol. 9 (4) (2010) 438–448.
[19] Y.R. Teo, D. Russell, S.S. Aphale, A.J. Fleming, Optimal integral force feedback and structured pi tracking control: application for high speed confocal microscopy, Mechatronics 24 (6) (2014) 701–711.
[20] J.L. Fanson, T.K. Caughey, Positive position feedback control for large space structures, AIAA J. 28 (4) (1990) 717–724.
[21] C.J. Goh, T.K. Caughey, On the stability problem caused by finite actuator dynamics in the collocated control of large space structures, Int. J. Control 41 (3) (1985) 787–802, http://dx.doi.org/10.1080/00207185089611 63.
[22] S.O.R. Moheimani, B.J.G. Vautier, B. Bhikkaji, Experimental implementation of extended multivariable PPF control on an active structure, IEEE Trans. Control Syst. Technol. 14 (3) (2006) 443–455.
[23] A. Mohammadi, A.G. Fowler, Y.K. Yong, S.O.R. Moheimani, A feedback controlled MEMS nanopositioner for on-chip high-speed AFM, IEEE J. Microelectromech. Syst. 23 (3) (2014) 610–619.
[24] H.R. Pota, S.O.R. Moheimani, M. Smith, Resonant controllers for smart structures, Smart Mater. Struct. 11 (1) (2002) 1–8.
[25] G.C. Goodwin, S.F. Graebe, M.E. Salgado, Control System Design, Prentice Hall International Inc., 2001.
[26] A.J. Fleming, Nanopositioning system with force feedback for high-performance tracking and vibration control, IEEE/ASME Trans. Mechatron. 15 (3) (2010) 433–447.
[27] A.J. Fleming, A review of nanometer resolution position sensors: operation and performance, Sens. Actuators A: Phys. 190 (2013) 106–126.
[28] Y.K. Yong, A. Fleming, S.O.R. Moheimani, A novel piezoelectric strain sensor for simultaneous damping and tracking control of a high-speed nanopositioner, IEEE/ASME Trans. Mechatron. 18 (3) (2013) 1113–1121.
[29] A.J. Fleming, A. Wills, S.O.R. Moheimani, Sensor fusion for improved control of piezoelectric tube scanners, IEEE Trans. Control Syst. Technol. 16 (6) (2008) 1265–1276.
[30] A.J. Fleming, B.J. Kenton, K.K. Leang, Bridging the gap between conventional and video-speed scanning probe microscopes, Ultramicroscopy 110 (9) (2010) 1205–1214.
[31] Y.K. Yong, S.O.R. Moheimani, Design of an inertially counterbalanced Z-nanopositioner for high-speed atomic force microscopy, IEEE/ASME Trans. Nanotechnol. 12 (2) (2013) 137–145.
[32] G. Schitter, W.F. Rijkee, N. Phan, Dual actuation for high-bandwidth nanopositioning, in: 47th IEEE Conference on Decision and Control, 2008. CDC 2008, 2008, pp. 5176–5181, http://dx.doi.org/10.1109/CDC.2008.4738876.
[33] A. Fleming, Dual-stage vertical feedback for high-speed scanning probe microscopy, IEEE Trans. Control Syst. Technol. 9 (1) (2011) 156–165.
[34] Y.K. Yong, B. Bhikkaji, S.O.R. Moheimani, Design, modeling and FPAA-based control of a high-speed atomic force microscope nanopositioner, IEEE/ASME Trans. Mechatron. 18 (3) (2013) 1060–1071.
[35] Y.K. Yong, A new preload mechanism for a high-speed piezoelectric stack nanopositioner, Mechatronics 36 (2016) 159–166, http://dx.doi.org/10.1016/j.mechatronics.2016.03.004.
[36] I. Petersen, A. Lanzon, Feedback control of negative-imaginary systems, IEEE Control Syst. Mag. 30 (5) (2010) 54–72.
[37] A.J. Fleming, Y.R. Teo, K.K. Leang, Low-order damping and tracking control for scanning probe systems, Front. Mech. Eng. 1 (2015) 1–9.
[38] A.J. Fleming, A method for measuring the resolution of nanopositioning systems, Rev. Sci. Instrum. 83 (8) (2012) 086101.

Biographies

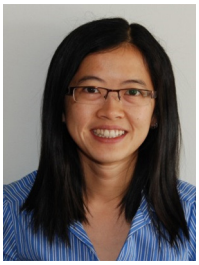

Yuen Kuan Yong received the B.Eng. degree (1st Class Hons.) in mechatronic engineering and the Ph.D. degree in mechanical engineering from The University of Adelaide, Australia, in 2001 and 2007, respectively. She is currently an Australian Research Council DECRA Fellow with the School of Electrical Engineering and Computer Science, The University of Newcastle, Australia. Her research interests include the design and control of nanopositioning systems, high-speed atomic force microscopy, finite-element analysis of smart materials and structures, sensing and actuation, and design and control of miniature robots. Dr. Yong is a recipient of the 2008 IEEE/ASME International Conference on Advanced Intelligent Mechatronics (AIM) Best Conference Paper Finalist Award, The University of Newcastle Vice-Chancellor's Awards for Research Excellence and the Pro Vice-Chancellor's Award for Excellence in Research Performance. She is an Associate Editor for Frontiers in Mechanical Engineering (specialty section Mechatronics) and the International Journal of Advanced Robotic Systems. She is also a steering committee member for the 2016 International Conference on Manipulation, Automation and Robotics at Small Scales (MARSS).

Andrew J. Fleming graduated from The University of Newcastle, Australia (Callaghan campus) with a Bachelor of Electrical Engineering in 2000 and Ph.D. in 2004. Dr. Fleming is presently an Australian Research Council Future Fellow and Director of the Precision Mechatronics Lab at The University of Newcastle, Australia. His research interests include biomedical devices, lithography, nanopositioning, and scanning probe microscopy. Dr. Fleming's research awards include the IEEE Transactions on Control Systems Technology Outstanding Paper Award and The University of Newcastle Researcher of the Year Award. He is the co-author of three books and more than 150 Journal and Conference articles. Dr. Fleming is the inventor of several patent applications, and in 2012 he received the Newcastle Innovation Rising Star Award for Excellence in Industrial Engagement.